

Design and Performance of the mDOM Mainboard for the IceCube Upgrade

The IceCube Collaboration

(a complete list of authors can be found at the end of the proceedings)

E-mail: karl-heinz.sulanke@desy.de, tba109@psu.edu,
jim.braun@icecube.wisc.edu

About 400 mDOMs (multi-PMT Digital Optical Modules) will be deployed as part of the IceCube Upgrade project. The mDOM's high pressure-resistant glass sphere houses 24 photomultiplier tubes (PMTs), 3 cameras, 10 flasher LEDs and various sensors. The mDOM mainboard design was challenging due to the limited available volume and demanding engineering requirements, like the maximum overall power consumption, a minimum trigger threshold of 0.2 photoelectrons (PE), the dynamic range and the linearity requirements. Another challenge was the FPGA firmware design, handling of about 35 Gbit/s of continuous ADC data from the digitization of the 24 PMT channels, the control of a high speed dynamic buffer and the discriminator output sampling rate of about 1 GSPS. High-speed sampling of each of the discriminator outputs at ~1 GSPS improves the leading-edge time resolution for the PMT waveforms. An MCU (microcontroller unit) coordinates the data taking, the data exchange with the surface and the sensor readout. Both the FPGA firmware and MCU software can be updated remotely. After discussing the main hardware blocks and the analog frontend (AFE) design, test results will be shown, covering especially the AFE performance. Additionally, the functionality of various sensors and modules will be evaluated.

Corresponding authors: K.-H. Sulanke^{1*}, T. Anderson², J. Braun³, A. Fienberg²

¹ *DESY, Zeuthen, Germany*

² *Dept. of Physics, Pennsylvania State University, University Park, USA*

³ *Dept. of Physics and Wisconsin IceCube Particle Astrophysics Center, University of Wisconsin-Madison, Madison, USA*

* Presenter

The 38th International Cosmic Ray Conference (ICRC2023)
26 July – 3 August, 2023
Nagoya, Japan



1. Introduction

The IceCube Upgrade detector [1] will be installed in the 2025/26 austral summer at the geographic South Pole in the center of the existing IceCube Neutrino Observatory. The IceCube Upgrade will enable precision measurements of neutrino properties, allow improved calibration of the IceCube array, and serve as a technology test platform for the future IceCube-Gen2 project. IceCube Upgrade will comprise about 700 optical sensors on seven strings. Among these sensors, 402 are mDOMs (multi-PMT Digital Optical Modules) [2]. Each mDOM features 24 3-inch photomultiplier tubes (PMTs), read out individually with a 120 MSPS 12-bit ADC. Single-channel triggers are realized with a per-channel discriminator, and nanosecond timing precision is achieved by sampling the discriminator output at 960 MSPS.

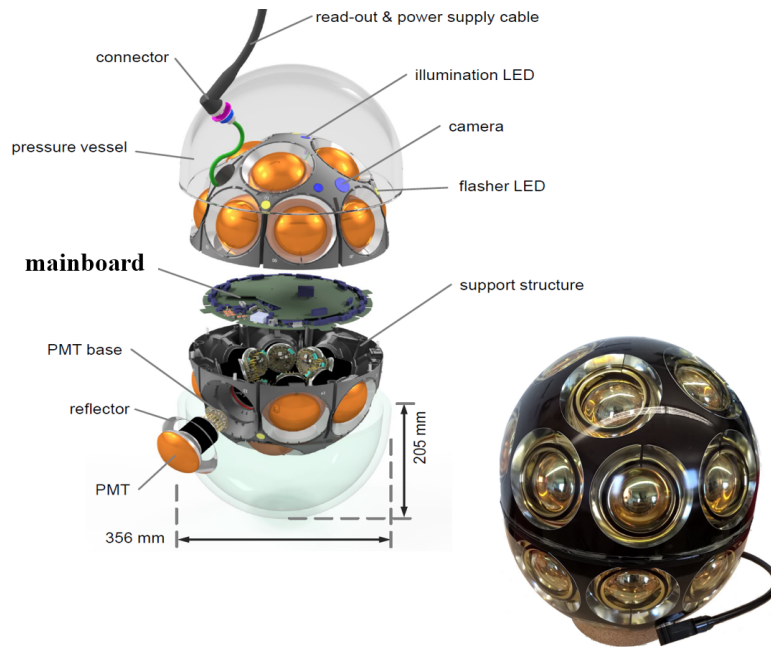


Figure 1: The IceCube Upgrade mDOM, exploded view (left) and photograph (right).

The mDOM mainboard is located in the “equatorial” region of the mDOM. See the exploded mDOM view in Fig. 1. The main components of the mDOM mainboard (Fig. 2) are two DC/DC converters, circuitry to monitor currents and voltages, 24 analog front-end (AFE) channels, a 2 Gbit DDR3-RAM-based event buffer, a powerful FPGA, an MCU (Microcontroller Unit), the ICM (IceCube Communication Module), a Xilinx CPLD, various sensors (Fig. 3) and the mDAB (mDOM Adapter Board, Fig. 8). When taking data at a sampling rate of 120 MSPS, the power consumption of the mDOM is about 9 W.

2. The Power Supplies

A single wire pair is being used to carry the DC power and communication signals of the mDOM. The isolating primary DC/DC converter, featuring a wide input range from 36 V to 160 V,

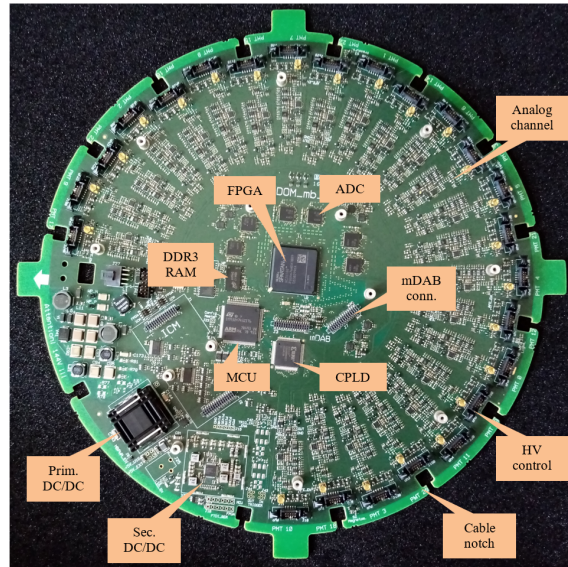


Figure 2: Photograph of an assembled mDOM mainboard, with major components labeled.

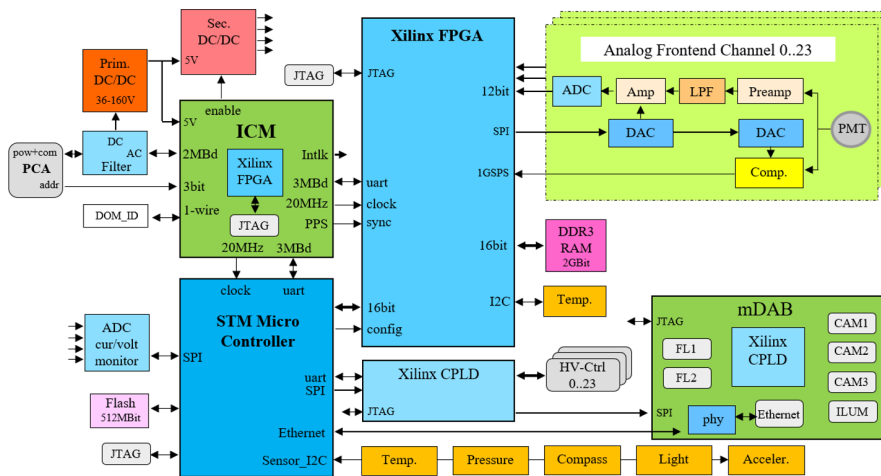


Figure 3: mDOM mainboard block diagram.

generates 5 V. The secondary DC/DC converter, an ADP5014ACPZ, converts the 5 V into four voltages of the range from 1 V to 3.3 V. It also controls the power on/off sequence of the four power rails (Fig. 4), like it is recommended for Xilinx Spartan 7 FPGAs.

Besides the proper on/off sequence, a very low noise level on the power rails is important as well, especially for the 1.8 V and the 3.3 V, partly being used to supply the analog frontend circuitry. An AC-coupled differential probe has been used to measure the noise levels (Fig. 5). For comparison the probe was shorted to GND first. The noise levels seen are very low, less than 2 mV pk-pk in a frequency range from DC to 1 GHz.

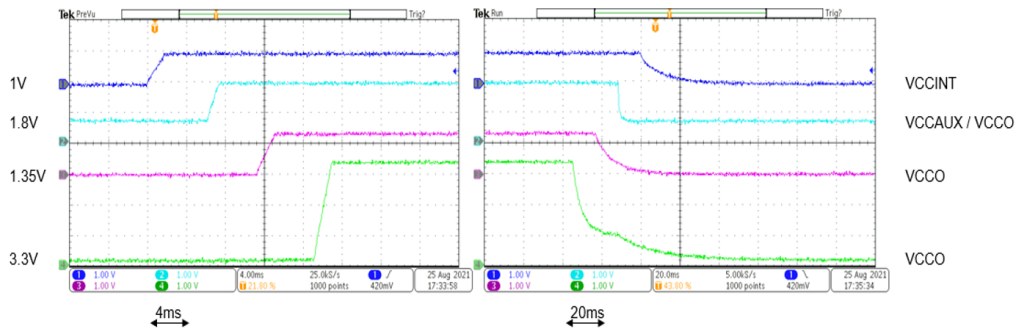


Figure 4: Secondary DC/DC converter, measured the power on/off sequence using a scope.

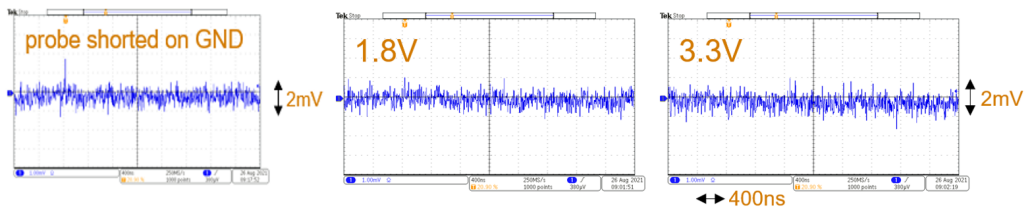


Figure 5: Secondary DC/DC converter, scope noise measurements on two analog voltage rails.

3. The ICM

The ICM (IceCube Communication Module, Fig. 6 left) is a universal piggy back module, being used by all IceCube Upgrade in-ice devices. A filter on the mainboard recovers the communication signal, modulated on the mDOM DC power. The primary component of the ICM is a Xilinx Spartan 7 FPGA. After power-on, the FPGA loads a write-protected “golden image”. Initiated by a software command, the FPGA loads a runtime image from another flash page afterwards. The runtime images can be remotely updated at any time. In case of a corrupted golden image, the FPGA tries to load a second, also write protected copy of the golden image. The ICM block diagram is shown in Fig. 6.

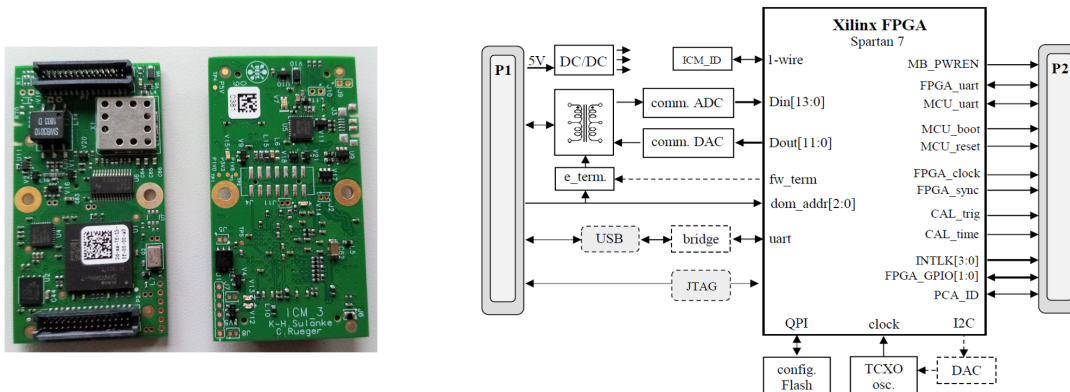


Figure 6: Photo and block diagram of the IceCube Communications Module (ICM).

After powering on a wire pair, only the ICM is powered on by default. Once the communication to the surface has been established, the next step is to enable the secondary DC/DC converter by an ICM command. Four interlock signals, like e.g. “High Voltage Enable”, are directly controlled by the ICM. A precision, low phase noise, temperature-compensated oscillator provides the 20 MHz system clock to the MCU and the FPGA. The low phase noise of the oscillator is important to guarantee the accurate time calibration, required for nanosecond-precision event timestamping. Data exchange, mainly between the ICM and the MCU, takes place through a UART channel running at 3 MBd.

The half-duplex communication signal is ASK-encoded. A trapezoidal-shaped bipolar pulse encodes a binary “1”, while a quiet line encodes a “0”. Figure 7 shows the 2 MBd communication signals, measured at both ends of a 2800 m-length IceCube cable.

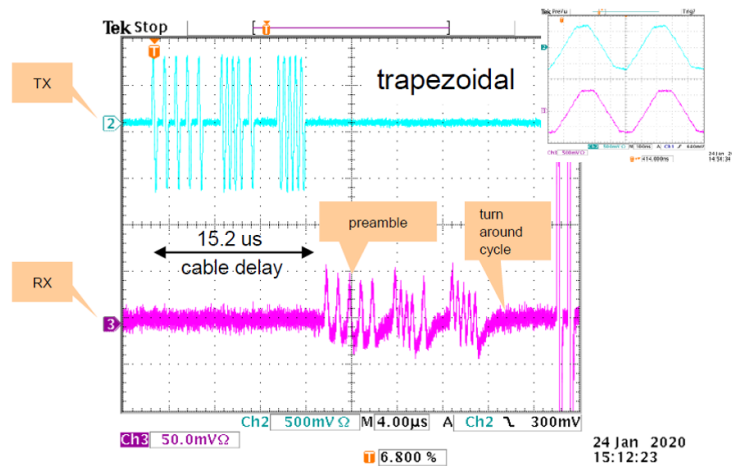


Figure 7: Wire pair communications signals at transmission (top) and reception (bottom) over a 2800 m-long cable.

4. The MCU

The microcontroller (MCU) is an STM32 of the type STM32H743ZIT6. Key features are a 32-bit Arm® Cortex®-M7 core with double-precision FPU, L1 cache (16 Kbytes of data and 16 Kbytes of instruction), a clock frequency up to 400 MHz, internal 2 Mbyte flash memory and 1 Mbyte RAM.

Once powered, the MCU boots from its flash, loading the mainboard FPGA afterwards. The FPGA is mapped into the MCU’s address range, like an external memory device, to be accessed via a 16-bit data bus. Before collecting event data, the MCU initializes the AFE channels and sets the high voltage of the PMTs. The PMT-base UART connection, multiplexed by a Xilinx CPLD to the MCU’s UART, allows setting and monitoring the PMT’s high voltage. An SPI bus is used to individually enable power to any of the AFE channels. The same bus also controls the mDAB board. A second SPI bus is used to gather power supply monitoring data. Temperature, pressure, compass, light and accelerometer sensors are controlled by an I²C bus. A 3 MBd UART connection is used for the data traffic to the ICM.

5. The mDAB

The mDOM Adapter Board (Fig. 8) is primarily needed to accommodate the connectors of three attached cameras, an illumination board and two LED flasher daisy chains. A Xilinx CPLD is translating the SPI bus commands of the MCU into power-enables and flasher-select signals. The ethernet connection is an option for test setups in the lab. Besides camera readout by SPI bus and flasher control, the mDAB also serves as a heat sink for the FPGA, lowering the FPGA-chip temperature by 10K. In addition the mDAB acts as a shield due to its GND-layer, protection the surrounding PMTs against EMI caused by the power supplies and the digital circuitry.

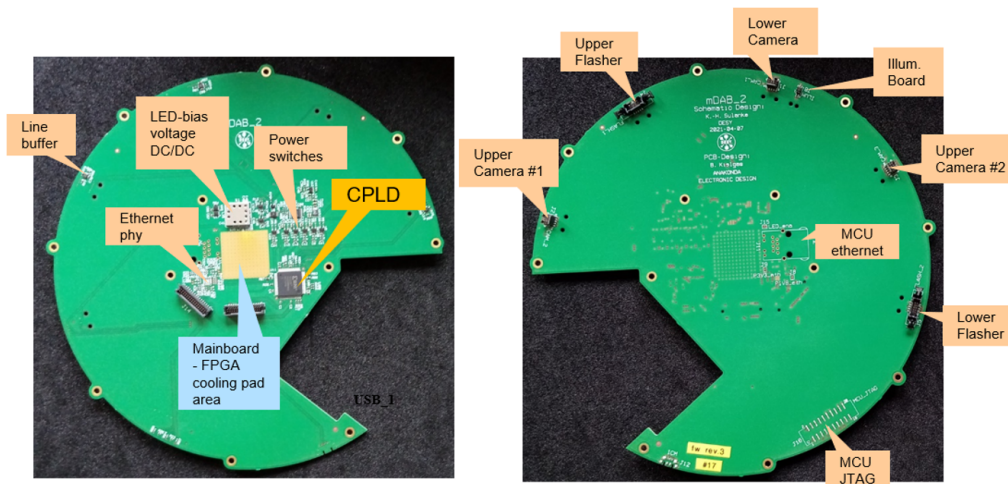


Figure 8: Photographs of the mDOM adapter board: bottom view (left) and top view (right).

6. The FPGA

The FPGA, a 676-pin BGA chip, is a Xilinx Spartan 7 XC7S100-2FGGA676I. Its main task is the readout of 24 analog front-end channels. The ADC baselines and trigger thresholds are set by the MCU through the FPGA. The serial ADC data, 48 serial bitstreams at 720 Mbit/s, result in an overall data rate of 34.56 Gbit/s. These bitstreams are continuously decoded and buffered. In case of a trigger, the corresponding data are propagated to the event buffer. The DDR3-RAM-based buffer, connected to the FPGA and organized as a ring buffer, allows the mDOM to store a sufficient amount of data to deal with any intermittent readout delays by the surface data acquisition software. The 24 ToT (time over threshold) signals, provided by the discriminators, are sampled at 960 MSPS, resulting in a leading-edge time resolution of about 1 ns.

7. The Analog Frontend

Most challenging for the analog frontend design was to accomplish a very low power consumption while maintaining enough bandwidth, sufficient dynamic range and a good linearity. Low noise in the neighborhood of EMI-causing digital parts like DC/DC converters, the MCU, the FPGA and

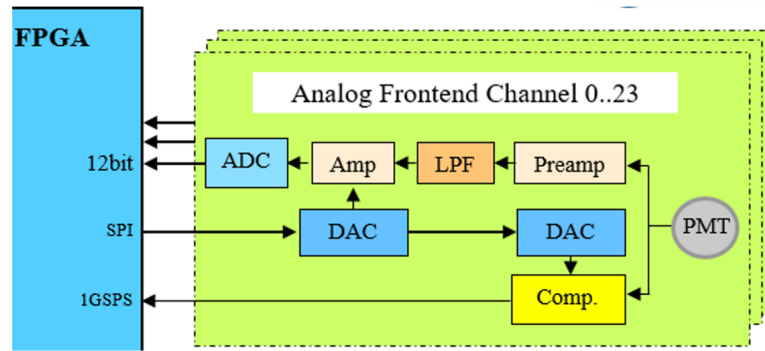


Figure 9: Block diagram of the Analog Frontend (AFE) circuit.

the DDR3 RAM was achieved by a careful design of the power supply and the PCB. The ADC baseline noise for all 24 channels is typically below 0.7 lsb RMS.

In contrast to traditional PMT readout designs with an AC-coupled input, we deal here with a fully DC-coupled approach. This avoids any signal droop effects (ADC-baseline variations) depending on the time between consecutive PMT pulses. Figure 9 shows the block diagram of the AFE. The PMT signal is directly connected to the discriminator (Comp.) and the preamplifier. Two precise 16-bit DAC channels are used to adjust the discriminator threshold and the ADC baseline. For pulse shaping a low pass filters is being used. Precision (0.1%) gain setting resistors are chosen. The dynamic range reaches from 0.2 PE to 150 PE. Figure 10 shows the comparison of simulation and measurement for a SPE-like pulse at an ADC sampling rate of 120 MSPS.

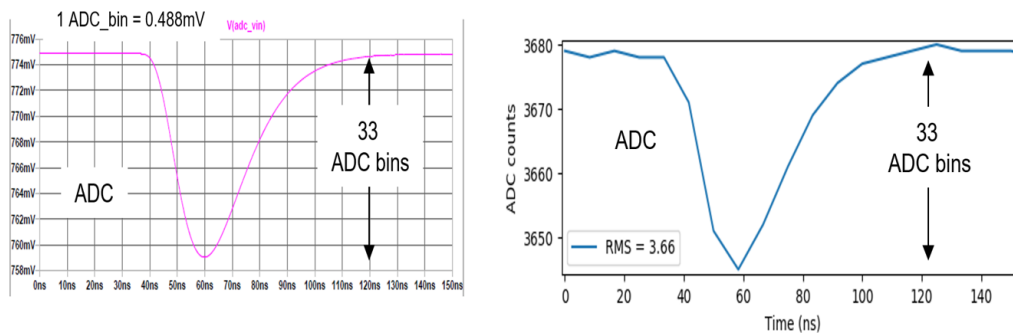


Figure 10: SPE like pulse, and simulated (left) and measured (right).

Figure 11 shows ADC readout and double pulse resolution of the discriminator for 0.2PE and 1PE signals. The double-pulse resolution of 10 nanoseconds is achievable by using the high-speed discriminator digitization even when the pulses are not separable in the filtered PMT signal.

Linearity measurements for the analog channel, using a calibrated laser source are depicted in Fig. 12. The required range was 100 PE. The saturation is caused by the AFE amplifiers.

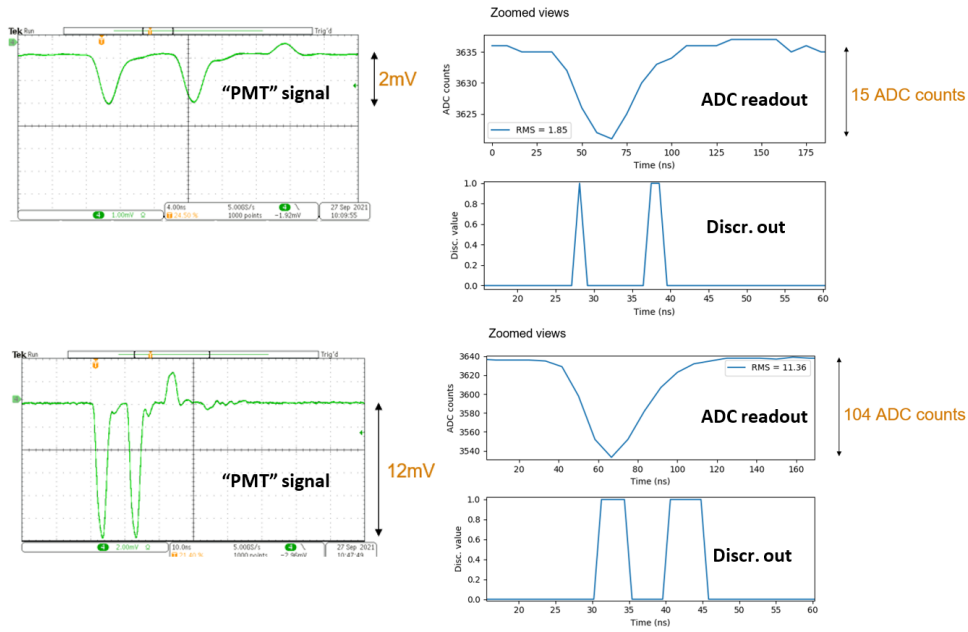


Figure 11: The PMT-pulse discriminator, 10 ns-double-pulse-resolution for 0.2 PE (top) and 1 PE (bottom).

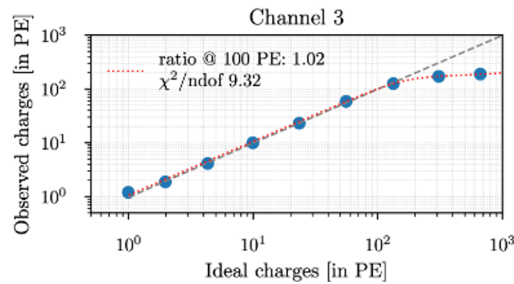


Figure 12: The AFE linearity measurement, using a calibrated laser source.

8. Conclusions and Status

The design fulfills the engineering requirements, e.g. operational temperature range, maximum AFE noise level, AFE linearity, data buffer size and event time resolution [3]. About 40 mDOM mainboards have been extensively tested so far. Each mainboard underwent a thermal shocks between -40°C and $+70^{\circ}\text{C}$. No failures have been observed after the stress tests. Presently the first batch of mainboards is being integrated into mDOMs, to be tested again during the final acceptance test (FAT) [3].

References

- [1] IceCube Collaboration *PoS ICRC2019* (2019) 1031.
- [2] IceCube Collaboration *PoS ICRC2021* (2021) 1070.
- [3] IceCube Collaboration *PoS ICRC2023* (these proceedings) 1183.

Full Author List: IceCube Collaboration

R. Abbasi¹⁷, M. Ackermann⁶³, J. Adams¹⁸, S. K. Agarwalla^{40, 64}, J. A. Aguilar¹², M. Ahlers²², J.M. Alameddine²³, N. M. Amin⁴⁴, K. Andeen⁴², T. Anderson⁵⁹, G. Anton²⁶, C. Argüelles¹⁴, Y. Ashida⁵³, S. Athanasiadou⁶³, S. N. Axani⁴⁴, X. Bai⁵⁰, A. Balagopal V.⁴⁰, M. Baricevic⁴⁰, S. W. Barwick³⁰, V. Basu⁴⁰, R. Bay⁸, J. J. Beatty^{20, 21}, J. Becker Tjus^{11, 65}, J. Beise⁶¹, C. Bellenghi²⁷, C. Benning¹, S. BenZvi⁵², D. Berley¹⁹, E. Bernardini⁴⁸, D. Z. Besson³⁶, E. Blaufuss¹⁹, S. Blot⁶³, F. Bontempo³¹, J. Y. Book¹⁴, C. Boscolo Meneguolo⁴⁸, S. Böser⁴¹, O. Botner⁶¹, J. Böttcher¹, E. Bourbeau²², J. Braun⁴⁰, B. Brinson⁶, J. Brostean-Kaiser⁶³, R. T. Burley², R. S. Busse⁴³, D. Butterfield⁴⁰, M. A. Campana⁴⁹, K. Carloni¹⁴, E. G. Carnie-Bronca², S. Chattopadhyay^{40, 64}, N. Chau¹², C. Chen⁶, Z. Chen⁵⁵, D. Chirkin⁴⁰, S. Choi⁵⁶, B. A. Clark¹⁹, L. Classen⁴³, A. Coleman⁶¹, G. H. Collin¹⁵, A. Connolly^{20, 21}, J. M. Conrad¹⁵, P. Coppin¹³, P. Correa¹³, D. F. Cowen^{59, 60}, P. Dave⁶, C. De Clercq¹³, J. J. DeLaunay⁵⁸, D. Delgado¹⁴, S. Deng¹, K. Deoskar⁵⁴, A. Desai⁴⁰, P. Desiati⁴⁰, K. D. de Vries¹³, G. de Wasseige³⁷, T. DeYoung²⁴, A. Diaz¹⁵, J. C. Díaz-Vélez⁴⁰, M. Dittmer⁴³, A. Domi²⁶, H. Dujmovic⁴⁰, M. A. DuVernois⁴⁰, T. Ehrhardt⁴¹, P. Eller²⁷, E. Ellinger⁶², S. El Mentawi¹, D. Elsässer²³, R. Engel^{31, 32}, H. Erpenbeck⁴⁰, J. Evans¹⁹, P. A. Evenson⁴⁴, K. L. Fan¹⁹, K. Fang⁴⁰, K. Farrag¹⁶, A. R. Fazely⁷, A. Fedynitch⁵⁷, N. Feigl¹⁰, S. Fiedlschuster²⁶, A. T. Fienberg⁵⁹, C. Finley⁵⁴, L. Fischer⁶³, D. Fox⁵⁹, A. Frackowiak¹¹, A. Fritz⁴¹, P. Fürst¹, J. Gallagher³⁹, E. Ganster¹, A. Garcia¹⁴, L. Gerhardt⁹, A. Ghadimi⁵⁸, C. Glaser⁶¹, T. Glauch²⁷, T. Glüsenskamp^{26, 61}, N. Goehlike³², J. G. Gonzalez⁴⁴, S. Goswami⁵⁸, D. Grant²⁴, S. J. Gray¹⁹, O. Gries¹, S. Griffin⁴⁰, S. Griswold⁵², K. M. Groth²², C. Günther¹, P. Gutjahr²³, C. Haack²⁶, A. Hallgren⁶¹, R. Halliday²⁴, L. Halve¹, F. Halzen⁴⁰, H. Hamdaoui⁵⁵, M. Ha Minh²⁷, K. Hanson⁴⁰, J. Hardin¹⁵, A. A. Harnisch²⁴, P. Hatch³³, A. Haungs³¹, K. Helbing⁶², J. Hellrung¹¹, F. Henningsen²⁷, L. Heuermann¹, N. Heyer⁶¹, S. Hickford⁶², A. Hidvegi⁵⁴, C. Hill¹⁶, G. C. Hill², K. D. Hoffman¹⁹, S. Hori⁴⁰, K. Hoshina^{40, 66}, W. Hou³¹, T. Huber³¹, K. Hultqvist⁵⁴, M. Hünnefeld²³, R. Hussain⁴⁰, K. Hyman²³, S. In⁵⁶, A. Ishihara¹⁶, M. Jacquart⁴⁰, O. Janik¹, M. Jansson⁵⁴, G. S. Japaridze⁵, M. Jeong⁵⁶, M. Jin¹⁴, B. J. P. Jones⁴, D. Kang³¹, W. Kang⁵⁶, X. Kang⁴⁹, A. Kappes⁴³, D. Kappesser⁴¹, L. Kardum²³, T. Karg⁶³, M. Karl²⁷, A. Karle⁴⁰, U. Katz²⁶, M. Kauer⁴⁰, J. L. Kelley⁴⁰, A. Khatee Zathul⁴⁰, A. Kheirandish^{34, 35}, J. Kiryluk⁵⁵, S. R. Klein^{8, 9}, A. Kochocki²⁴, R. Koirala⁴⁴, H. Kolanoski¹⁰, T. Kontrims²⁷, L. Köpke⁴¹, C. Kopper²⁶, D. J. Koskinen²², P. Koundal³¹, M. Kovacevich⁴⁹, M. Kowalski^{10, 63}, T. Kozynets²², J. Krishnamoorthi^{40, 64}, K. Kruijswijk³⁷, E. Krupczak²⁴, A. Kumar⁶³, E. Kun¹¹, N. Kurahashi⁴⁹, N. Lad⁶³, C. Lagunas Gualda⁶³, M. Lamoureux³⁷, M. J. Larson¹⁹, S. Latseva¹, F. Lauber⁶², J. P. Lazar^{14, 40}, J. W. Lee⁵⁶, K. Leonard DeHolton⁶⁰, A. Leszczyńska⁴⁴, M. Lincetto¹¹, Q. R. Liu⁴⁰, M. Liubarska²⁵, E. Lohfink⁴¹, C. Love⁴⁹, C. J. Lozano Mariscal⁴³, L. Lu⁴⁰, F. Lucarelli²⁸, W. Luszczak^{20, 21}, Y. Lyu^{8, 9}, J. Madsen⁴⁰, K. B. M. Mahn²⁴, Y. Makino⁴⁰, E. Manao²⁷, S. Mancina^{40, 48}, W. Marie Sainte⁴⁰, I. C. Mariş¹², S. Marka⁴⁶, Z. Marka⁴⁶, M. Marsee⁵⁸, I. Martinez-Soler¹⁴, R. Maruyama⁴⁵, F. Mayhew²⁴, T. McElroy²⁵, F. McNally³⁸, J. V. Mead²², K. Meagher⁴⁰, S. Mechbal⁶³, A. Medina²¹, M. Meier¹⁶, Y. Merckx¹³, L. Merten¹¹, J. Micallef²⁴, J. Mitchell⁷, T. Montaruli²⁸, R. W. Moore²⁵, Y. Morii¹⁶, R. Morse⁴⁰, M. Moulai⁴⁰, T. Mukherjee³¹, R. Naab⁶³, R. Nagai¹⁶, M. Nakos⁴⁰, U. Naumann⁶², J. Necker⁶³, A. Negi⁴, M. Neumann⁴³, H. Niederhausen²⁴, M. U. Nisa²⁴, A. Noell¹, A. Novikov⁴⁴, S. C. Nowicki²⁴, A. Obertacke Pollmann¹⁶, V. O'Dell⁴⁰, M. Oehler³¹, B. Oeyen²⁹, A. Olivias¹⁹, R. Ørsøe²⁷, J. Osborn⁴⁰, E. O'Sullivan⁶¹, H. Pandya⁴⁴, N. Park³³, G. K. Parker⁴, E. N. Paudel⁴⁴, L. Paul^{42, 50}, C. Pérez de los Heros⁶¹, J. Peterson⁴⁰, S. Philippen¹, A. Pizzuto⁴⁰, M. Plum⁵⁰, A. Pontén⁶¹, Y. Popovych⁴¹, M. Prado Rodriguez⁴⁰, B. Pries²⁴, R. Procter-Murphy¹⁹, G. T. Przybylski⁹, C. Raab³⁷, J. Rack-Helleis⁴¹, K. Rawlins³, Z. Rechav⁴⁰, A. Rehman⁴⁴, P. Reichherzer¹¹, G. Renzi¹², E. Resconi²⁷, S. Reusch⁶³, W. Rhode²³, B. Riedel⁴⁰, A. Rifaie¹, E. J. Roberts², S. Robertson^{8, 9}, S. Rodan⁵⁶, S. Roellinghoff⁵⁶, M. Rongen²⁶, C. Rot^{53, 56}, T. Ruhe²³, L. Ruohan²⁷, D. Ryckbosch²⁹, I. Safa^{14, 40}, J. Saffer³², D. Salazar-Gallegos²⁴, P. Sampathkumar³¹, S. E. Sanchez Herrera²⁴, A. Sandrock⁶², M. Santander⁵⁸, S. Sarkar²⁵, S. Sarkar⁴⁷, J. Savelberg¹, P. Savina⁴⁰, M. Schaufel¹, H. Schieler³¹, S. Schindler²⁶, L. Schlickmann¹, B. Schlüter⁴³, F. Schlüter¹², N. Schmeisser⁶², T. Schmidt¹⁹, J. Schneider²⁶, F. G. Schröder^{31, 44}, L. Schumacher²⁶, G. Schwefer¹, S. Sclafani¹⁹, D. Seckel⁴⁴, M. Seikh³⁶, S. Seunarine⁵¹, R. Shah⁴⁹, A. Sharma⁶¹, S. Shefali³², N. Shimizu¹⁶, M. Silva⁴⁰, B. Skrzypek¹⁴, B. Smithers⁴, R. Snihur⁴⁰, J. Soedingrekso²³, A. Sjøgaard²², D. Soldin³², P. Soldin¹, G. Sommani¹¹, C. Spannfellner²⁷, G. M. Spiczak⁵¹, C. Spiering⁶³, M. Stamatikos²¹, T. Stanev⁴⁴, T. Stezelberger⁹, T. Stürwald⁶², T. Stuttard²², K.-H. Sulanke⁶³, G. W. Sullivan¹⁹, I. Taboada⁶, S. Ter-Antonyan⁷, M. Thiesmeyer¹, W. G. Thompson¹⁴, J. Thwaites⁴⁰, S. Tilav⁴⁴, K. Tollefson²⁴, C. Tönnes⁵⁶, S. Toscano¹², D. Tosi⁴⁰, A. Trettin⁶³, C. F. Tung⁶, R. Turcotte³¹, J. P. Twagirayezu²⁴, B. Ty⁴⁰, M. A. Unland Elorrieta⁴³, A. K. Upadhyay^{40, 64}, K. Upshaw⁷, N. Valtonen-Mattila⁶¹, J. Vandenbroucke⁴⁰, N. van Eijndhoven¹³, D. Vannerom¹⁵, J. van Santen⁶³, J. Vara⁴³, J. Veitch-Michaelis⁴⁰, M. Venugopal³¹, M. Vereecken³⁷, S. Verpoest⁴⁴, D. Veske⁴⁶, A. Vijai¹⁹, C. Walck⁵⁴, C. Weaver²⁴, P. Weigel¹⁵, A. Weindl³¹, J. Weldert⁶⁰, C. Wendt⁴⁰, J. Werthebach²³, M. Weyrauch³¹, N. Whitehorn²⁴, C. H. Wiebusch¹, N. Willey²⁴, D. R. Williams⁵⁸, L. Witthaus²³, A. Wolf¹, M. Wolf²⁷, G. Wrede²⁶, X. W. Xu⁷, J. P. Yanez²⁵, E. Yildizci⁴⁰, S. Yoshida¹⁶, R. Young³⁶, F. Yu¹⁴, S. Yu²⁴, T. Yuan⁴⁰, Z. Zhang⁵⁵, P. Zhelnin¹⁴, M. Zimmerman⁴⁰

¹ III. Physikalisches Institut, RWTH Aachen University, D-52056 Aachen, Germany

² Department of Physics, University of Adelaide, Adelaide, 5005, Australia

³ Dept. of Physics and Astronomy, University of Alaska Anchorage, 3211 Providence Dr., Anchorage, AK 99508, USA

⁴ Dept. of Physics, University of Texas at Arlington, 502 Yates St., Science Hall Rm 108, Box 19059, Arlington, TX 76019, USA

⁵ CTSPS, Clark-Atlanta University, Atlanta, GA 30314, USA

⁶ School of Physics and Center for Relativistic Astrophysics, Georgia Institute of Technology, Atlanta, GA 30332, USA

⁷ Dept. of Physics, Southern University, Baton Rouge, LA 70813, USA

⁸ Dept. of Physics, University of California, Berkeley, CA 94720, USA

⁹ Lawrence Berkeley National Laboratory, Berkeley, CA 94720, USA

¹⁰ Institut für Physik, Humboldt-Universität zu Berlin, D-12489 Berlin, Germany

¹¹ Fakultät für Physik & Astronomie, Ruhr-Universität Bochum, D-44780 Bochum, Germany

¹² Université Libre de Bruxelles, Science Faculty CP230, B-1050 Brussels, Belgium

- ¹³ Vrije Universiteit Brussel (VUB), Dienst ELEM, B-1050 Brussels, Belgium
¹⁴ Department of Physics and Laboratory for Particle Physics and Cosmology, Harvard University, Cambridge, MA 02138, USA
¹⁵ Dept. of Physics, Massachusetts Institute of Technology, Cambridge, MA 02139, USA
¹⁶ Dept. of Physics and The International Center for Hadron Astrophysics, Chiba University, Chiba 263-8522, Japan
¹⁷ Department of Physics, Loyola University Chicago, Chicago, IL 60660, USA
¹⁸ Dept. of Physics and Astronomy, University of Canterbury, Private Bag 4800, Christchurch, New Zealand
¹⁹ Dept. of Physics, University of Maryland, College Park, MD 20742, USA
²⁰ Dept. of Astronomy, Ohio State University, Columbus, OH 43210, USA
²¹ Dept. of Physics and Center for Cosmology and Astro-Particle Physics, Ohio State University, Columbus, OH 43210, USA
²² Niels Bohr Institute, University of Copenhagen, DK-2100 Copenhagen, Denmark
²³ Dept. of Physics, TU Dortmund University, D-44221 Dortmund, Germany
²⁴ Dept. of Physics and Astronomy, Michigan State University, East Lansing, MI 48824, USA
²⁵ Dept. of Physics, University of Alberta, Edmonton, Alberta, Canada T6G 2E1
²⁶ Erlangen Centre for Astroparticle Physics, Friedrich-Alexander-Universität Erlangen-Nürnberg, D-91058 Erlangen, Germany
²⁷ Technical University of Munich, TUM School of Natural Sciences, Department of Physics, D-85748 Garching bei München, Germany
²⁸ Département de physique nucléaire et corpusculaire, Université de Genève, CH-1211 Genève, Switzerland
²⁹ Dept. of Physics and Astronomy, University of Gent, B-9000 Gent, Belgium
³⁰ Dept. of Physics and Astronomy, University of California, Irvine, CA 92697, USA
³¹ Karlsruhe Institute of Technology, Institute for Astroparticle Physics, D-76021 Karlsruhe, Germany
³² Karlsruhe Institute of Technology, Institute of Experimental Particle Physics, D-76021 Karlsruhe, Germany
³³ Dept. of Physics, Engineering Physics, and Astronomy, Queen's University, Kingston, ON K7L 3N6, Canada
³⁴ Department of Physics & Astronomy, University of Nevada, Las Vegas, NV, 89154, USA
³⁵ Nevada Center for Astrophysics, University of Nevada, Las Vegas, NV 89154, USA
³⁶ Dept. of Physics and Astronomy, University of Kansas, Lawrence, KS 66045, USA
³⁷ Centre for Cosmology, Particle Physics and Phenomenology - CP3, Université catholique de Louvain, Louvain-la-Neuve, Belgium
³⁸ Department of Physics, Mercer University, Macon, GA 31207-0001, USA
³⁹ Dept. of Astronomy, University of Wisconsin–Madison, Madison, WI 53706, USA
⁴⁰ Dept. of Physics and Wisconsin IceCube Particle Astrophysics Center, University of Wisconsin–Madison, Madison, WI 53706, USA
⁴¹ Institute of Physics, University of Mainz, Staudinger Weg 7, D-55099 Mainz, Germany
⁴² Department of Physics, Marquette University, Milwaukee, WI, 53201, USA
⁴³ Institut für Kernphysik, Westfälische Wilhelms-Universität Münster, D-48149 Münster, Germany
⁴⁴ Bartol Research Institute and Dept. of Physics and Astronomy, University of Delaware, Newark, DE 19716, USA
⁴⁵ Dept. of Physics, Yale University, New Haven, CT 06520, USA
⁴⁶ Columbia Astrophysics and Nevis Laboratories, Columbia University, New York, NY 10027, USA
⁴⁷ Dept. of Physics, University of Oxford, Parks Road, Oxford OX1 3PU, United Kingdom
⁴⁸ Dipartimento di Fisica e Astronomia Galileo Galilei, Università Degli Studi di Padova, 35122 Padova PD, Italy
⁴⁹ Dept. of Physics, Drexel University, 3141 Chestnut Street, Philadelphia, PA 19104, USA
⁵⁰ Physics Department, South Dakota School of Mines and Technology, Rapid City, SD 57701, USA
⁵¹ Dept. of Physics, University of Wisconsin, River Falls, WI 54022, USA
⁵² Dept. of Physics and Astronomy, University of Rochester, Rochester, NY 14627, USA
⁵³ Department of Physics and Astronomy, University of Utah, Salt Lake City, UT 84112, USA
⁵⁴ Oskar Klein Centre and Dept. of Physics, Stockholm University, SE-10691 Stockholm, Sweden
⁵⁵ Dept. of Physics and Astronomy, Stony Brook University, Stony Brook, NY 11794-3800, USA
⁵⁶ Dept. of Physics, Sungkyunkwan University, Suwon 16419, Korea
⁵⁷ Institute of Physics, Academia Sinica, Taipei, 11529, Taiwan
⁵⁸ Dept. of Physics and Astronomy, University of Alabama, Tuscaloosa, AL 35487, USA
⁵⁹ Dept. of Astronomy and Astrophysics, Pennsylvania State University, University Park, PA 16802, USA
⁶⁰ Dept. of Physics, Pennsylvania State University, University Park, PA 16802, USA
⁶¹ Dept. of Physics and Astronomy, Uppsala University, Box 516, S-75120 Uppsala, Sweden
⁶² Dept. of Physics, University of Wuppertal, D-42119 Wuppertal, Germany
⁶³ Deutsches Elektronen-Synchrotron DESY, Platanenallee 6, 15738 Zeuthen, Germany
⁶⁴ Institute of Physics, Sachivalaya Marg, Sainik School Post, Bhubaneswar 751005, India
⁶⁵ Department of Space, Earth and Environment, Chalmers University of Technology, 412 96 Gothenburg, Sweden
⁶⁶ Earthquake Research Institute, University of Tokyo, Bunkyo, Tokyo 113-0032, Japan

Acknowledgements

The authors gratefully acknowledge the support from the following agencies and institutions: USA – U.S. National Science Foundation-Office of Polar Programs, U.S. National Science Foundation-Physics Division, U.S. National Science Foundation-EPSCoR, Wisconsin Alumni Research Foundation, Center for High Throughput Computing (CHTC) at the University of Wisconsin–Madison, Open Science

Grid (OSG), Advanced Cyberinfrastructure Coordination Ecosystem: Services & Support (ACCESS), Frontera computing project at the Texas Advanced Computing Center, U.S. Department of Energy-National Energy Research Scientific Computing Center, Particle astrophysics research computing center at the University of Maryland, Institute for Cyber-Enabled Research at Michigan State University, and Astroparticle physics computational facility at Marquette University; Belgium – Funds for Scientific Research (FRS-FNRS and FWO), FWO Odysseus and Big Science programmes, and Belgian Federal Science Policy Office (Belspo); Germany – Bundesministerium für Bildung und Forschung (BMBF), Deutsche Forschungsgemeinschaft (DFG), Helmholtz Alliance for Astroparticle Physics (HAP), Initiative and Networking Fund of the Helmholtz Association, Deutsches Elektronen Synchrotron (DESY), and High Performance Computing cluster of the RWTH Aachen; Sweden – Swedish Research Council, Swedish Polar Research Secretariat, Swedish National Infrastructure for Computing (SNIC), and Knut and Alice Wallenberg Foundation; European Union – EGI Advanced Computing for research; Australia – Australian Research Council; Canada – Natural Sciences and Engineering Research Council of Canada, Calcul Québec, Compute Ontario, Canada Foundation for Innovation, WestGrid, and Compute Canada; Denmark – Villum Fonden, Carlsberg Foundation, and European Commission; New Zealand – Marsden Fund; Japan – Japan Society for Promotion of Science (JSPS) and Institute for Global Prominent Research (IGPR) of Chiba University; Korea – National Research Foundation of Korea (NRF); Switzerland – Swiss National Science Foundation (SNSF); United Kingdom – Department of Physics, University of Oxford.